

Uniform asymptotic Green's functions for efficient modeling of cracks in elastic layers with relative shear deformation controlled by linear springs

Anthony P. Peirce^{1,*†}, Hongren Gu² and Eduard Siebrits³

¹Department of Mathematics, University of British Columbia, Vancouver, BC, Canada

²Schlumberger IPC, Sugar Land, TX, U.S.A.

³Schlumberger Moscow Research, Moscow, Russia

SUMMARY

We present a uniform asymptotic solution (UAS) for a displacement discontinuity (DD) that lies within the middle layer of a three-layer elastic medium in which relative shear deformation between parallel interfaces is controlled by linear springs. The DD is assumed to be normal to the two interfaces between the elastic media. Using the Fourier transform method we construct a leading term in the asymptotic expansion for the spectral coefficient functions for a DD in a three-layer-spring medium. Although a closed-form solution will require a solution in terms of an infinite series, we demonstrate how this UAS can be used to construct highly efficient and accurate solutions even in the case in which the DD actually touches the interface. We compare the results using the Green's function UAS solution for a crack crossing a soft interface with results obtained using a multi-layer boundary element method. We also present results from an implementation of the UAS Green's function approach in a pseudo-3D hydraulic fracturing simulator to analyze the effect of interface shear deformation on the fracture propagation process. These results are compared with field measurements. Copyright © 2008 John Wiley & Sons, Ltd.

Received 12 October 2007; Revised 31 December 2007; Accepted 3 March 2008

KEY WORDS: uniform asymptotic solutions; interfaces with relative shear deformation; cracks in layered elastic media; Fourier transforms

1. INTRODUCTION

The accurate and efficient solution to fracture propagation problems in layered elastic media is of considerable importance in a number of engineering applications such as pavement design, stress analysis of mining excavations, and hydraulic fracturing. The particular application of interest in this paper involves the modeling of a hydraulic fracture. Hydraulic fracturing is a process by which

*Correspondence to: Anthony P. Peirce, Department of Mathematics, University of British Columbia, Vancouver, BC, Canada.

†E-mail: peirce@math.ubc.ca

a crack is forced to propagate in an assumed elastic medium by the injection of a viscous fluid under high pressure. Hydraulic fractures occur naturally when pressurized magma flows cause fractures to propagate deep in the earth's crust. In the petroleum industry, hydraulic fractures are deliberately created in oil and gas reservoirs to substantially enhance production. It is important to be able to model the evolution of these propagating fractures in order to control their location within the reservoir by adjusting the available engineering parameters. Such a design tool can, for example, be used to prevent the fractures from breaking out of the so-called pay zone into an unproductive zone that may be saturated with water.

Models of hydraulic fractures typically assume that the fluid flow along the crack surface can be adequately represented by lubrication theory; the rock mass is represented by a layered elastic medium comprising piecewise homogeneous layers separated by parallel interfaces across which neighboring distinct elastic materials are bonded; the fractures are assumed to take the orientation of least resistance and evolve within a plane that is perpendicular to the direction of the minimum principal geological stress; the fracture growth is controlled by the principles of linear elastic fracture mechanics in which the stress intensity factor at any point at the fracture tip is assumed to be in equilibrium with the local toughness of the rock. In spite of these simplifying assumptions, the models typically involve a degenerate coupled system of integro-partial differential equations that are defined on a domain with a free boundary. However, such simplified models are naturally idealizations of complex field situations that are approximated either for computational convenience or for lack of adequate physical models. Focusing on examples of complexity in field situations that have been ignored in the modeling of the solid rock mass, the rock may be naturally fractured; it may be subject to plastic deformations; the layers may not be parallel; or they may slip allowing interface shear deformation. It is this latter complexity that this paper is aimed at addressing. Indeed, we present a model of interface shear deformation in which the pack of elastic layers is coupled by linear springs. The assumption of linear springs is introduced in order to maintain an elasticity description that is still linear in order to make it possible to construct a Green's function for this layer-spring medium. The use of linear interface conditions to model the shear deformation across interfaces in layered elastic media is not new. Indeed, linear models of interface deformation have been used in models of surface subsidence [1], in the analysis of deformations in layered pavements subjected to surface loads [2], in the modeling of hydraulic fracturing in layered elastic materials [3], and more recently in the analysis of multilayer piezothermoelastic plates with imperfect interfaces [4]. The novelty of the technique presented here is the uniform asymptotic solution (UAS) approach, which is crucial to the efficient and accurate modeling of cracks that cross the interfaces undergoing shear deformation.

One of the key ingredients in a hydraulic fracture simulator is a robust and efficient technique to solve for the crack-opening displacement for a prescribed pressure on the surfaces of a fracture in an infinite-layered elastic medium. Although a number of numerical techniques are available to achieve this, each has its own advantages and disadvantages. The finite element method or the finite difference method can easily treat variations in the elastic properties and even plastic behavior. These volume-based methods require an adequate discretization of the 3D infinite elastic medium either by truncation of the domain or by deploying infinite elements. In addition, in order to capture the expected singular behavior in the vicinity of the fracture tip specialized singular elements are required. Since the fracture footprint is not known *a priori* these techniques will require remeshing and interpolation of field quantities for each new location of the fracture footprint. By contrast, a standard boundary element method (BEM) [5] requires only discretization of the crack plane as well as the layer interfaces. The BEM is most efficient for the treatment of piecewise

uniform elastic media—the treatment of arbitrary inhomogeneities or plastic behavior requires the evaluation of costly volume integrals.

A layer Green's function approach [6–8], which has been particularly effective in the modeling of hydraulic fractures for the case of bonded interfaces, makes use of a semi-analytic technique based on the Fourier transform (FT) method to construct the influence function matrix for elemental displacement discontinuities within a layered elastic medium. Although this technique is a BEM, it is not standard in that the construction of the layer Green's function enables one to avoid the additional computational burden of discretizing the layer interfaces as is required by the standard BEM. In order to model a fracture that crosses bonded interfaces, a crucial component is the UAS (see [6]) for a displacement discontinuity (DD) element that is located within an elastic layer that is bonded to and sandwiched between two elastic half-spaces. In this paper, we present the UAS for a DD element located within an elastic layer that is sandwiched between two elastic half-spaces and connected by linear springs. This Green's function can then be used to generate an efficient model for the evolution of a hydraulic fracture within a layered elastic medium in which interface shear deformation is possible. Although the DD element in this paper is assumed to be perpendicular to the layer interfaces, the UAS technique can also be extended to consider a DD element that has an arbitrary inclination to the two parallel interfaces that bound the elastic layer in which it is located.

A fixed, Eulerian mesh comprising a network of rectangular DD elements is defined. This mesh is typically chosen to have sufficient resolution to capture early fracture footprints while still incorporating a sufficient area to be able to enclose the fracture evolution over the desired time frame. The Green's function influence matrix associated with this mesh is then constructed *a priori* and used repeatedly as the fracture evolves. The existence of the Green's function for this layer-spring medium rests on the assumption of linear springs that control the interface shear deformation, which makes it possible to determine the influence of all the active DD elements by superposition. Modeling more complex, nonlinear interface deformation or frictional sliding would rule out the possibility of using superposition via a Green's function and would necessitate the solution to the full 3D nonlinear boundary value problem for each new trial pressure field.

In Section 2, we define the geometry and the properties of the layer-spring system and briefly summarize the governing equations and the FT technique used to reduce the elastic partial differential equations to systems of ordinary differential equations (ODEs). In Section 3, we present the 2D and 3D UASs in the wave number domain and briefly describe the process of inversion of the UAS for the 2D case. In Section 4, we provide some numerical results. Firstly, we compare the solution for a pressurized crack that crosses two interfaces using the UAS algorithm to that using a 2D multilayer BEM. Secondly, we implement the layer-spring multilayer Green's function approach in a pseudo-3D (P3D) hydraulic fracture simulator. In a case study, the Renshaw and Pollard criterion [9] is used to identify interfaces that exhibit relative shear deformation thereby terminating fracture height growth, and shear deformation along these interfaces is modeled using a layer Green's function with a reduced interface stiffness.

2. GOVERNING EQUATIONS AND LAYER-SPRING GEOMETRY

2.1. An elastic material in 3D

Consider a linear elastic material that occupies a region in a 3D space and which is in a state of equilibrium. In this case, the stresses σ_{ij} and the strains $\epsilon_{ij} = 1/2(u_{i,j} + u_{j,i})$, which are defined

in terms of the displacement gradients $u_{i,j} = \partial u_i / \partial x_j$ at any point within the body, satisfy the following partial differential equations:

$$\sigma_{ij} = \lambda \varepsilon_{kk} \delta_{ij} + 2G \varepsilon_{ij} \quad (1)$$

$$\sigma_{ij,j} + f_i = 0 \quad (2)$$

where λ and G are Lamé's constants that can be expressed in terms of Young's modulus E and Poisson's ratio ν of the material by the formulae $\lambda = E\nu/(1+\nu)(1-2\nu)$ and $G = E/2(1+\nu)$ and f_i are the applied body forces. Following [10] it is convenient to introduce the constants a , b , and f that are defined by $a = \lambda + 2G$, $b = \lambda$, and $f = 2G$.

It is also useful in this context, in which the layer properties do not change in the x - and z -directions but do vary in the y -direction (see Figure 1); to rewrite the system equations (1) and (2) in the form of a system in which the x - and z -derivatives have been separated from the y -derivatives:

$$\partial_y T = \mathcal{A}T + F \quad (3)$$

where T represents the vector of stresses and displacements defined by

$$T = [\sigma_{yy} \ \sigma_{xy} \ \sigma_{yz} \ u_y \ u_x \ u_z]^T$$

the body force vector is given by $F = [-f_y \ -f_x \ -f_z \ 0 \ 0 \ 0]^T$, and \mathcal{A} is the differential operator involving only x - and z -derivatives, which is defined by

$$\mathcal{A} = \begin{bmatrix} 0 & -\partial_x & -\partial_z & 0 & 0 & 0 \\ -\frac{b}{a}\partial_x & 0 & 0 & 0 & \left(\frac{(b^2-a^2)}{a}\right)\partial_{xx} - \frac{f}{2}\partial_{zz} & \left(\frac{(b^2-ab)}{a} - \frac{f}{2}\right)\partial_{xz} \\ -\frac{b}{a}\partial_z & 0 & 0 & 0 & \left(\frac{(b^2-ab)}{a} - \frac{f}{2}\right)\partial_{xz} & \left(\frac{(b^2-a^2)}{a}\right)\partial_{zz} - \frac{f}{2}\partial_{xx} \\ \frac{1}{a} & 0 & 0 & 0 & -\frac{b}{a}\partial_x & -\frac{b}{a}\partial_z \\ 0 & \frac{2}{f} & 0 & -\partial_x & 0 & 0 \\ 0 & 0 & \frac{2}{f} & -\partial_z & 0 & 0 \end{bmatrix} \quad (4)$$

2.2. Geometry of the elastic layers and layer-spring conditions

In this section we introduce the geometry and labeling convention that we will assume for the elastic medium, and describe the interface deformation conditions. We assume that the body is divided into N layers in which the moduli can be different (see Figure 1). Depending on the problem being considered, the pack of N layers can either extend to ∞ in both directions or there can be a free surface on the top of the pack of layers, which rests on an elastic half-space (as is shown in Figure 1). We assign numbers to the layers starting from layer $[1]$ for the bottom half-space and ending with layer number $[N]$ for the top layer adjacent to the free surface. These layer

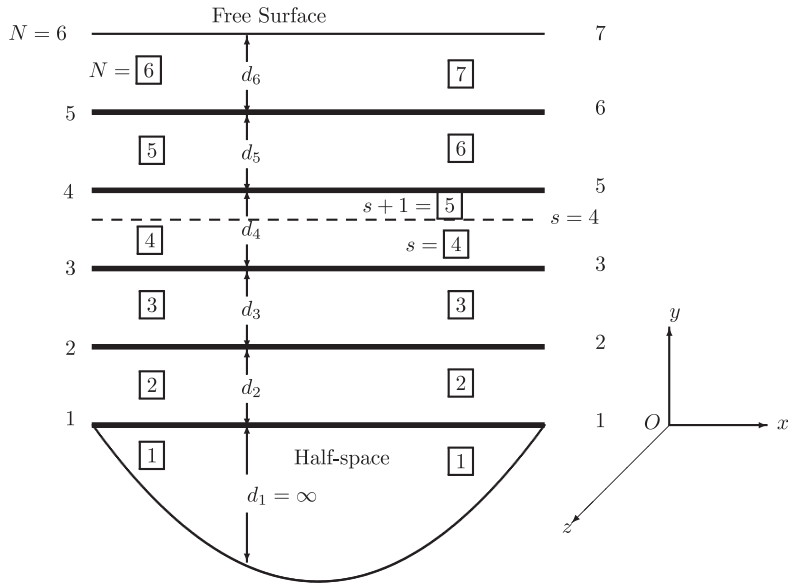


Figure 1. Geometry and labeling of a stack of elastic layers that sit on an elastic half-space. Shear deformation across interfaces between the layers is controlled by linear springs, whereas the normal deformation and shear and normal tractions are continuous. The interfaces with springs are represented by thick lines.

indices are represented by the boxed sequence of numbers on the left side of Figure 1. The layer interfaces are numbered in a similar manner and the corresponding sequence of interface indices for this problem are shown on the extreme left-hand side of Figure 1. Observe that the interface at the top of a layer has the same index as the layer itself. The thicknesses of the layers \$d_i\$, which may all be distinct, are also shown in the figure. Similarly, the symbols \$E_i\$ and \$v_i\$ are used to denote the elastic moduli of the \$i\$th layer. We introduce a Cartesian coordinate system \$Oxyz\$ in which the \$x\$- and \$z\$-axes are aligned with the horizontal layers and in which the \$y\$-coordinate is measured upwards from the interface between the pack of layers and the bottom half-space (see Figure 1).

Point displacement or force discontinuities can be introduced into the \$N\$-layer elastic medium by specifying appropriate jump conditions in the stress and displacement fields across a horizontal layer having the same \$y\$ coordinate as the desired source point. This is achieved by introducing a pseudo-interface, which is represented by the dashed line through layer [4] in Figure 1. This process divides layer [4] into two layers for the purposes of this source computation and increases the number of layers by one. For the purposes of the computation the layers are renumbered using the same procedure as before and the layer numbers and interface indices are shown on the right-hand side of Figure 1. The symbol \$s\$ will be reserved for the \$[s]\$th layer immediately below the pseudo-'source' interface.

The elastic layers are connected at their interfaces by linear springs that satisfy the following conditions:

$$\begin{aligned} \Delta\sigma_{yy} &= 0, & \Delta\sigma_{yx} &= 0, & \Delta\sigma_{yz} &= 0 \\ \Delta u_y &= 0, & \sigma_{yx} &= S_i \Delta u_x, & \sigma_{yz} &= S_i \Delta u_z \end{aligned} \quad (5)$$

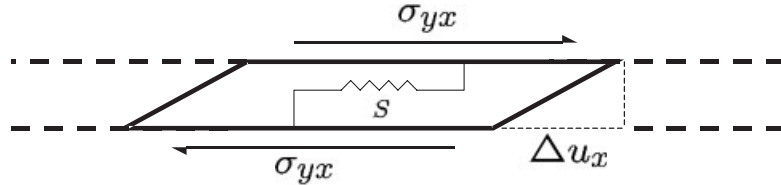


Figure 2. Interface deformation Δu_x in response to a shear stress of σ_{yx} that is applied across an interface between two elastic layers that are connected by a spring of stiffness S .

where $\Delta\sigma_{kl}$ and Δu_k , respectively, represent the jumps in the stress and displacement components across the interface and $S_i \geq 0$ is the stiffness constant associated with the i th interface. The stress continuity conditions in (5) express the equilibrium of forces across the interface, whereas the continuity in the y -displacement component expresses the vertical compatibility between the elastic layers. The linear relations between the interface shear stresses and the corresponding shear deformations characterize the linear elastic springs. The situation in which the interfaces are perfectly bonded corresponds to the case $S_i \rightarrow \infty$ in which case the displacement jumps are forced to be zero, i.e. $\Delta u_x = 0 = \Delta u_z$. The layer deformation corresponding to the relation $\sigma_{yx} = S_i \Delta u_x$ is depicted in Figure 2.

2.3. Reduction of the layer PDEs to a system of ODEs

Since we have assumed that the material properties do not vary in the x - and z -directions we can apply the 2D FT (see [6, 7, 10–17]) to the system of Equations (3) to obtain

$$\partial_y \widehat{T} = \widehat{\mathcal{A}} \widehat{T} + \widehat{F} \quad (6)$$

where $\widehat{\mathcal{A}}$ is defined to be

$$\widehat{\mathcal{A}} = \begin{bmatrix} 0 & -k & 0 & 0 & 0 & 0 \\ \frac{b}{a}k & 0 & 0 & \frac{(a^2 - b^2)}{a}k^2 & 0 & 0 \\ \frac{1}{a} & 0 & 0 & -\frac{b}{a}k & 0 & 0 \\ 0 & \frac{2}{f} & k & 0 & 0 & 0 \\ 0 & 0 & 0 & 0 & 0 & \frac{f}{2}k \\ 0 & 0 & 0 & 0 & \frac{2}{f} & 0 \end{bmatrix} \quad (7)$$

and where $k = (m^2 + n^2)^{1/2}$ and m and n are the x and z wave numbers, respectively. In (7) the elements of \widehat{T} and \widehat{F} have been arranged as follows:

$$\widehat{T} = [\widehat{\sigma}_{yy}, \widehat{\tau}_s, \widehat{u}_y, \widehat{u}_s, \widehat{\tau}_t, \widehat{u}_t]^T \quad \text{and} \quad \widehat{F} = [-\widehat{f}_y, -\widehat{f}_s, 0, 0, -\widehat{f}_t, 0]^T$$

Here we have followed [10] and [6, 7] by defining the displacement and stress components of \widehat{T} to be

$$\begin{aligned}\widehat{u}_s &= -i(m\widehat{u}_x + n\widehat{u}_z)/k \\ \widehat{u}_t &= -i(m\widehat{u}_x - n\widehat{u}_z)/k\end{aligned}\quad (8)$$

and

$$\begin{aligned}\widehat{\tau}_s &= -i(m\widehat{\sigma}_{xy} + n\widehat{\sigma}_{yz})/k \\ \widehat{\tau}_t &= -i(n\widehat{\sigma}_{xy} - m\widehat{\sigma}_{yz})/k\end{aligned}\quad (9)$$

We observe from (7) that unknowns involving $\widehat{\sigma}_{yy}$, $\widehat{\tau}_s$, \widehat{u}_y , and \widehat{u}_s (the s -subsystem) are completely de-coupled from the unknowns involving $\widehat{\tau}_t$ and \widehat{u}_t (the t -subsystem). The s -subsystem is sufficient to determine boundary value problems for 2D plane strain, whereas the autonomous t -subsystem is the only additional part that needs to be added to the plane strain equations in order to determine boundary value problems in 3D. We note that by setting either $m=0$ or $n=0$ we obtain the corresponding plane strain equations with the out-of-plane direction being the x - (or, respectively, the z -) direction.

Combining the interface conditions (5) with the definitions of s and t displacements and stresses (8) and (9), we obtain the following transformed interface conditions:

$$\widehat{\tau}_s = S_i \Delta \widehat{u}_s \quad \text{and} \quad \widehat{\tau}_t = S_i \Delta \widehat{u}_t$$

2.4. Layer ODE solution, spectral coefficients, and spring layer difference equations

Considering the wave number k as a parameter, we can now determine the solution to the system of ODEs (6), which can be expressed in terms of the solutions for the s -subsystem and the t -subsystem as follows (see [10]):

$$\begin{bmatrix} T_s \\ T_t \end{bmatrix} = \begin{bmatrix} Z_s & 0 \\ 0 & Z_t \end{bmatrix} \begin{bmatrix} A_s \\ A_t \end{bmatrix} \quad (10)$$

where

$$\begin{aligned}T_s &= [\widehat{\sigma}_{yy}^l/k \ \widehat{\tau}_s^l/k \ \widehat{u}_y^l \ \widehat{u}_s^l]^T, \quad A_s = [A_1 \ A_2 \ A_3 \ A_4]^T \\ T_t &= [\widehat{\tau}_t^l/k \ \widehat{u}_t^l]^T, \quad A_t = [A_5 \ A_6]^T \\ Z_s &= \begin{bmatrix} -f e^{-ky} & (l_4 - fky)e^{-ky} & f e^{ky} & (l_4 + fky)e^{ky} \\ -f e^{-ky} & (l_5 - fky)e^{-ky} & -f e^{ky} & -(l_5 + fky)e^{ky} \\ e^{-ky} & kye^{-ky} & e^{ky} & kye^{ky} \\ e^{-ky} & (ky - l_2)e^{-ky} & -e^{ky} & -(ky + l_2)e^{ky} \end{bmatrix}\end{aligned}$$

and

$$Z_t = \begin{bmatrix} -\frac{f}{2} e^{-ky} & \frac{f}{2} e^{ky} \\ e^{-ky} & e^{ky} \end{bmatrix}$$

and the constants l_j in (10) are defined as follows:

$$l_2 = \frac{\lambda+3G}{\lambda+G}, \quad l_4 = \frac{2G^2}{\lambda+G}, \quad l_5 = \frac{2G(\lambda+2G)}{\lambda+G} \quad (11)$$

2.5. Spectral coefficient algebraic equations and source DD

For a well-posed boundary value problem, the exact solution to (6) in each of the layers is used to construct a system of algebraic equations for the layer spectral coefficients $A_j^l(k)$, which express the conditions that prevail at the layer interfaces. Here $A_j^l(k)$ represents the j th spectral coefficient, as defined in (10), for the l th layer associated with the wave number k . For the spring layer system, these algebraic equations are constructed by using the interface jump equations (5) to obtain the following interface conditions for the s -system:

$$0 = \begin{bmatrix} [\hat{\sigma}_{yy}]_l^{l+1}/k \\ [\hat{\tau}_s]_l^{l+1}/k \\ [\hat{u}_y]_l^{l+1} \\ [\hat{u}_s]_l^{l+1} - \frac{1}{S_l} \hat{\tau}_s \end{bmatrix} = \begin{bmatrix} Z_{1,s}^{l+1} A_s^{l+1} - Z_{1,s}^l A_s^l \\ Z_{2,s}^{l+1} A_s^{l+1} - Z_{2,s}^l A_s^l \\ Z_{3,s}^{l+1} A_s^{l+1} - Z_{3,s}^l A_s^l \\ (Z_{4,s}^{l+1} A_s^{l+1} - Z_{4,s}^l A_s^l) - \frac{k}{S_l} Z_{4,s}^l A_s^l \end{bmatrix}$$

and the following interface conditions for the t -system:

$$0 = \begin{bmatrix} [\hat{\tau}_t]_l^{l+1}/k \\ [\hat{u}_t]_l^{l+1} - \frac{1}{S_l} \hat{\tau}_t \end{bmatrix} = \begin{bmatrix} Z_{1,t}^{l+1} A_t^{l+1} - Z_{1,t}^l A_t^l \\ (Z_{2,t}^{l+1} A_t^{l+1} - Z_{2,t}^l A_t^l) - \frac{k}{S_l} Z_{2,t}^l A_t^l \end{bmatrix}$$

Here $Z_{j,s}^{l+1}$ is the j th row of the Z_s matrix for the $l+1$ st layer and $Z_{j,t}^{l+1}$ is the j th row of the Z_t matrix for the $l+1$ st layer.

For a pack containing both very thick and thin layers, the elements of the matrices Z_s^l and Z_t^l involve exponentials of large quantities and, as a result, the system of algebraic equations for the $A_s^l(k)$ and $A_t^l(k)$ that result from the direct application of (10) becomes poorly conditioned. In this case it is necessary to reformulate the algebraic equations as a well-conditioned system of difference equations (see [7, 18] for details of this procedure) involving the following pressure quantities at the top of each layer:

$$p^i = \begin{bmatrix} \hat{\sigma}_{yy}/k \\ \hat{\tau}_s/k \end{bmatrix} \text{ at the top of the } i\text{th layer for the } s\text{-system}$$

$$p^i = \hat{\tau}_t/k \text{ at the top of the } i\text{th layer for the } t\text{-system}$$

In order to implement interface springs, the layer difference equations can be expressed in the form

$$0 = R_{bt}^{i+1} p^{i+1} + (R_{bb}^{i+1} - R_{tt}^i - \Sigma^i) p^i - R_{tb}^i p^{i-1} \quad (12)$$

where the flexibility matrices R_{bt}^{i+1} , R_{bb}^{i+1} , R_{tt}^i , and R_{tb}^i are given in Appendix A and

$$\Sigma^i = \begin{bmatrix} 0 & 0 \\ 0 & \frac{1}{S_i} \end{bmatrix} \text{ for the } s\text{-system and } \Sigma^i = \frac{1}{S_i} \text{ for the } t\text{-system}$$

It can be shown [19] that a normal point vertical DD located at y_s with a displacement jump Δu in the z -direction can be represented by stress-traction discontinuities across the plane $y=y_s$ of the following form:

$$[\widehat{T}(y_s)] = \begin{bmatrix} 0 \\ \Delta u(b^2 - a^2)/a \\ \Delta u b/a \\ 0 \\ 0 \\ 0 \end{bmatrix} + \frac{m^2}{(m^2 + n^2)} \begin{bmatrix} 0 \\ \Delta u(a - b) \\ 0 \\ 0 \\ 0 \\ 0 \end{bmatrix} + \frac{mn}{(m^2 + n^2)} \begin{bmatrix} 0 \\ 0 \\ 0 \\ 0 \\ 0 \\ \Delta u(a - b) \end{bmatrix} \quad (13)$$

The first forcing vector on the right-hand side of (13) is precisely the same one that appears in plane strain problems and only acts on the s -system and we will refer to the solutions obtained using this forcing as the P_s solution. The second forcing vector is in the form of a forcing on the s -subsystem and we will refer to this as the Ancillary s -solution, which we will denote by the A_s solution. The third vector is in the form of a forcing on the t -subsystem and we refer to this Ancillary solution as the A_t solution. Because the dependence on m and n can be factored out of each of these forcing vectors, we can determine the solution for the forcing vectors without the factors involving m and n , and then we can multiply these solutions by the appropriate functions of m and n in order to get the required solution for any given wave number pair (m, n) .

3. UNIFORM ASYMPTOTIC SOLUTIONS

3.1. UASs in the wave number domain

In order to determine the numerical Green's function for a DD in a layered elastic material it is necessary (see [6]) to make use of a three-layer asymptotic solution in which the source DD is located in the middle layer of a three-layer elastic medium. This three-layer solution (called the UAS in [6]) is then used to remove the high wave number components from the spectral coefficients before they are inverted by numerical integration to obtain the stress and displacement influences in real space. Since the system is linear, the stress and displacement components of the UAS are then added to the inverted low-frequency components to yield the complete DD stress and displacement components. This solution is crucial in the situation in which DD influences are to be used to model a crack that crosses one or more interfaces. In this case, significant high wave number components have to be removed from the spectral coefficients in order to make numerical inversion feasible. In this section, we describe the form of the spectral coefficients $A_j^{l,\mu}(k)$ for the UAS for a three-layer elastic medium in which two elastic half-spaces are joined to an elastic layer (see Figure 3). Coupling between the layers assumes that across the interfaces

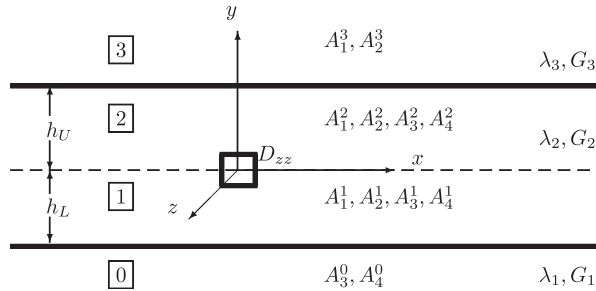


Figure 3. A vertical DD in an elastic layer that is joined to two elastic half-spaces by linear springs that control the shear deformation across the interfaces (represented by the thick horizontal lines). The normal displacement fields are compatible across the interfaces, whereas the normal and shear tractions are continuous to ensure force equilibrium.

between the layers the shear and normal tractions are continuous (which guarantees equilibrium), that the normal deformations are continuous, whereas linear springs control the shear deformation across the interfaces between the layers. We use the exact solutions for two coupled half-planes to derive the uniformly valid leading-order asymptotic approximation to the spectral coefficients for the three-layer problem.

If the vertical DD falls in the region where $h_L \ll h_U$, the three-layer solution will tend, for large k values, to the solution for a vertical DD in the upper part of two half-planes that are joined by springs, whereas if the DD falls in the region where $h_L \gg h_U$, the three-layer solution will tend, for large k values, to the solution for a vertical DD in the lower part of two half-planes that are joined by springs. If, on the other hand, the DD is not much closer to one interface than the other so that $h_L \sim h_U$, then as $k \rightarrow \infty$ the ultimate asymptotic solution is the solution for a vertical DD in an infinite medium to which both the upper and lower solutions tend. Thus, we have a typical situation that occurs in the asymptotic analysis (see, for example, [20]), in which two different asymptotic solutions are valid in different regions but they are both valid in a finite overlap region that they both share. In this case, it is possible to obtain an asymptotic approximation that is uniformly valid over the three regions by superimposing the two asymptotic solutions and subtracting the solution in the match region:

$$A_j^{l,\mu}(k) \xrightarrow{k \rightarrow \infty} A_j^{l,U}(k) + A_j^{l,L}(k) - A_j^{l,\infty}(k) \quad (14)$$

where $A_j^{l,\mu}(k)$ is used to represent the uniformly valid asymptotic solution, $A_j^{l,U}(k)$ represents the corresponding spectral coefficient for two half-spaces connected by linear springs in which the interface is above the source DD, $A_j^{l,L}(k)$ represents the corresponding half-space spectral coefficient in which the spring interface is below the source DD, and $A_j^{l,\infty}(k)$ represents the spectral coefficient for a point vertical DD in an infinite medium having the material properties λ_2 and G_2 of the middle layer.

The explicit expressions for the uniform asymptotic spectral coefficients $A_j^{l,Ps\mu}(k)$, $A_j^{l,As\mu}(k)$, $A_j^{l,At\mu}(k)$ that are calculated by substituting the respective expressions for: $A_j^{l,PsU}(k)$, $A_j^{l,PsL}(k)$, and $A_j^{l,Ps\infty}(k)$; $A_j^{l,AsU}(k)$, $A_j^{l,AsL}(k)$, and $A_j^{l,As\infty}(k)$; and $A_j^{l,AtU}(k)$, $A_j^{l,AtL}(k)$, and $A_j^{l,At\infty}(k)$

into (14) are given in Appendix B. Generically the UAS coefficients are of the form

$$A_j^{l,\mu}(k) = \sum_s g_s^Q(k)$$

where the functions $g_s^Q(k)$ are rational functions of the wave number k of the form

$$g_s^{Q_i}(k) = \frac{c_1^{s,i}k + c_2^{s,i}h_i k^2 + c_3^{s,i}h_i^2 k^3 + \sigma_i[\bar{c}_0^{s,i} + \bar{c}_1^{s,i}(h_i k) + \bar{c}_2^{s,i}(h_i k)^2]}{k + \beta_i \sigma_i} e^{-2kh_i} \quad (15)$$

where the coefficients c_p^s can be expressed in terms of the parameters $\varepsilon_i = G_i/G_2$, $\delta_i = \lambda_i/\lambda_2$, $\sigma_i = S_i/G_2$, and $\rho = \lambda_2/G_2$. The exponential factor e^{-2kh_i} may or may not be present depending upon whether the term represents an image element or not. We note that if we consider the limit $\sigma_i \rightarrow \infty$, the rational functions are reduced to polynomials in k in which the coefficients $\bar{c}_p^{s,i}/\beta_i$ are the same as those that were obtained for the fully bonded layers [6]. We recover the fully bonded coefficients in this limit, as expected, since an infinitely stiff interface spring is equivalent to a fully bonded interface.

3.2. Inversion of the UAS

In order to invert the FTs of the influences and to construct integrated kernels we follow the approach described in [6]. In order to make it possible to use the spectral method to determine the spatial influences of the singular case, in which a crack intersects the interface between two layers, it is necessary to first subtract the uniform asymptotic spectral coefficients $A_j^{l,\mu}(k)$ presented in Appendix B from the numerical spectral coefficients $A_j^l(k)$. The numerical coefficients are obtained by solving the block-tridiagonal system of linear equations (12) that corresponds to the geometry and interface conditions for the problem under consideration. We then obtain a set of low-frequency components $A_j^{l,\mathcal{L}}(k)$ that are used in the numerical inversion process, i.e.

$$A_j^{l,\mathcal{L}}(k) = A_j^l(k) - A_j^{l,\mu}(k) \quad (16)$$

Since $A_j^l(k) \xrightarrow{k \rightarrow \infty} A_j^{l,\mu}(k)$, it follows that $A_j^{l,\mathcal{L}}(k) \xrightarrow{k \rightarrow \infty} 0$. If the uniform asymptotic approximation closely mimics the true solution, then $A_j^{l,\mathcal{L}}(k)$ will only be non-zero for relatively low frequencies. After subtracting the asymptotic solution, the remaining spectral coefficients $A_j^{l,\mathcal{L}}(k)$ that need to be inverted contain only relatively low-frequency components. As a result, it is possible to invert the low-frequency spectra $A_j^{l,\mathcal{L}}(k)$ very efficiently using numerical integration. The high-frequency components that are associated with the UAS $A_j^{l,\mu}(k)$ cannot be inverted numerically. However, these uniform spectral coefficients can be inverted analytically to yield approximate spatial stress and displacement components due to a point vertical DD in a three-layer material.

As we observed in the last section, the difference between the spectral coefficients for the fully bonded and the spring layer system is that the fully bonded coefficients involve polynomials in k whereas the spring layer system involves rational functions in k (see (15)). By using synthetic division it is possible to reduce all the integrands to the same form as those required in the bonded

case given in [6], except for the remainder term. For example, the remainder term in the 2D case involves an inversion integral of the form

$$\begin{aligned} I_{-1}(y') &= \frac{1}{\pi} \int_0^\infty \frac{e^{-|k|y'}}{b+k} dk \\ &= \frac{1}{\pi} e^{by'} E_1(by') \end{aligned}$$

where

$$E_1(s) = \int_s^\infty \frac{e^{-t}}{t} dt = -\text{Ei}(-s)$$

and Ei is the exponential integral. To complete the computation of the spatial UAS due to a piecewise constant DD, for example, involves evaluating integrals involving the product of $I_{-1}(y')$ and powers of y' up to degree 2. These integrals are given in Appendix C.

3.3. The numerical procedure to solve crack problems

The pressurized crack problem is conveniently expressed [5] in the form of an integral equation:

$$\int_{R(t)} C(x, y; \xi, \eta) w(\xi, \eta, t) d\xi d\eta = p(x, y, t)$$

where w is the unknown width (DD) profile within the crack and p is the prescribed net pressure within the crack.

The given fracture geometry is discretized into M elements—line segments in 2D and rectangular elements in 3D. Each of the DD elements of the discretized problem is assumed to send a set of stress influences to each of the other receiving elements in the mesh. These stress influences are determined by adding the integrated uniform stress components $\sigma_{zz}^{l,\mu}$ and the integrated low-frequency stress components $\sigma_{zz}^{l,\mathcal{L}}$ at receiving points located at the centers of the receiving elements. Assembling all possible send–receive pairs of influences and storing them in a matrix C , we obtain the following discrete form of the above crack integral equation:

$$\sum_{n=1}^M C_{mn} w_n = p_m$$

3.4. Implementation in a hydraulic fracture simulator

Interfacial slip is one of the mechanisms that arrests fracture height growth in hydraulic fracturing. To model hydraulic fracturing in formations with interfacial slip, the plane strain (2D) UAS method described above is implemented in a P3D hydraulic fracture simulator [21]. In the simulator, the bedding interfaces are assumed to be horizontal and parallel to each other, and the hydraulic fracture is vertical and is perpendicular to the direction of the minimum horizontal *in situ* stress. Relative shear deformation across an interface directly affects the fracture height growth in the vertical direction and the fracture width profile. Since hydraulic fracturing is a coupled process between the fracture deformation and the fluid flow inside the fracture, the fracture height and width are influenced by the interfacial slip, which can affect the overall fracture pressure and

geometry. The UAS method is used to calculate the fracture width profile along the fracture height due to the fluid pressure inside the fracture. In addition to the UAS method, we also need a fracture height growth criterion to determine when interfacial slip occurs. We use the Renshaw and Pollard criterion [9] to determine if fracture propagation will occur across frictional interfaces. The criterion was derived for cohesionless interfaces. In hydraulic fracturing, however, if the fracturing fluid penetrates between bedding layers, the cohesion of the interface would be much weakened and the Renshaw and Pollard criterion could be used as a first-order approximation to identify whether fracture crossing will occur or not. For the coordinate system shown in Figure 1, the Renshaw and Pollard criterion is given by

$$\frac{-\sigma'_{yy}}{T_0 - \sigma'_{xx}} > \frac{0.35 + \frac{0.35}{\mu}}{1.06} \quad (17)$$

where $\sigma'_{yy} = \sigma_{yy} - p_0$ is the effective vertical overburden *in situ* stress, $\sigma'_{xx} = \sigma_{xx} - p_0$ is the effective minimum horizontal *in situ* stress, p_0 is the pore pressure, T_0 is the rock tensile strength, and μ is the coefficient of friction of the interface. The vertical stress σ_{yy} acts perpendicular to the interface, and the horizontal stress σ_{xx} can be discontinuous across the interface and the value used in the criterion is the one in the layer into which the fracture may further propagate after crossing the interface. According to this criterion, when the condition in (17) is satisfied, there is no interfacial slip and the hydraulic fracture can cross the interface. If the condition in (17) is not satisfied for a particular interface, then interfacial slip is assumed to occur and the hydraulic fracture is assumed to terminate at the interface.

The numerical implementation in a P3D simulator follows the procedure described in [21]. The main difference is in the building of the fracture width, height, area, and pressure tables used in the simulator. Since the parameters involved in (17) are only dependent on the local geological stress state and material properties, it is possible to test the different interfaces in a particular field situation for the potential slip. First, we determine whether a bedding interface allows hydraulic fracture crossing based on criterion (17). For an interface where the criterion indicates fracture crossing, the conventional fracture height growth criterion

$$K_I = K_{Ic} \quad (18)$$

is applied and a large value of shear stiffness S is allocated for the perfectly bonded interface. For an interface where criterion (17) indicates relative slip deformation, the fracture height growth is limited and a small value (determined by user) is used for the shear stiffness S for that interface. The small interface stiffness allocated to interfaces with relative slip makes it possible to account for any interface shear deformation that might take place automatically within the layer Green's function. According to the procedure described in [21], this is achieved by using the UAS method to calculate tables for the fracture width, height, and cross-sectional area corresponding to various pressures. These tables are then used to determine the fracture height and geometry within a hydraulic fracture simulation. Simulation results for a field example are presented in the following section.

4. NUMERICAL RESULTS

In this section we provide some numerical results to illustrate the use of the method outlined above.

4.1. A pressurized crack crossing two deforming interfaces

In this subsection we consider the problem of determining the opening displacement of a crack subjected to an internal pressure of 10 MPa. The crack is located within the interval $x=0$ and $0.5 < y < 3.5$ m and crosses two soft interfaces in a pack of elastic layers that are joined by linear springs. To demonstrate the effect of layer stiffness we present results in which the crack intersects layers with the following distinct stiffnesses: 1, 2, and 4 GPa/m. The geometry of the layers, the location of the crack, and material properties are shown in Figure 4.

The solution obtained using the FT algorithm described above is compared with the solution obtained using a DD BEM [22]. The FT algorithm was implemented by discretizing the crack into 60 piecewise constant DD elements. Because the Green's function matrix already incorporates the effect of the linear springs and the free surface, there was no need to discretize along the layer interfaces. The BEM algorithm used 2730 piecewise linear DD elements to discretize the crack, the four interfaces with linear springs, and the free surface. Since there are two collocation points per DD element this solution comprises 5460 degrees of freedom compared with the 60 degrees of freedom required by the UAS layer Green's function algorithm. The solutions generated by these two algorithms are compared in Figure 5. There is close agreement between the solutions generated by the two algorithms. Due to the relaxation in shear stress by the deformation of the

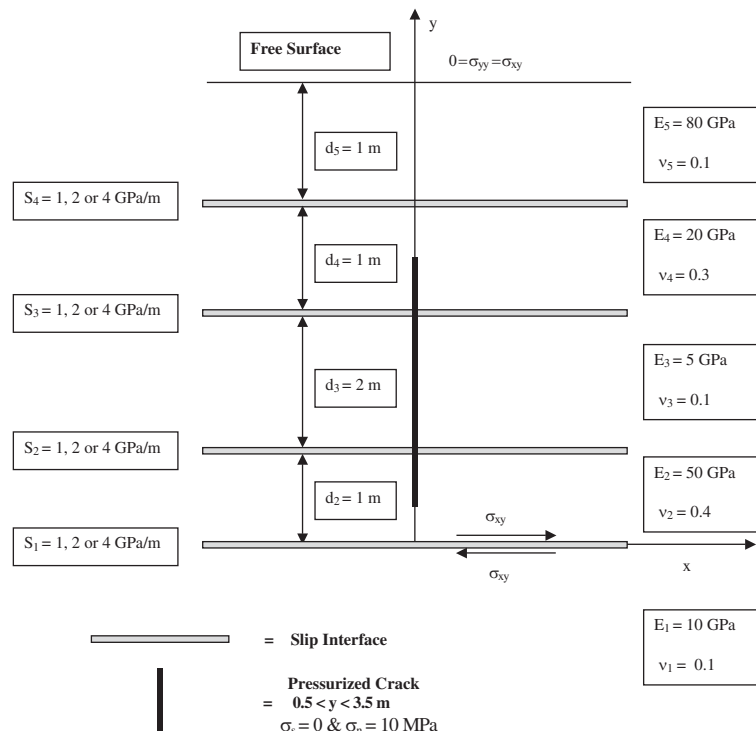


Figure 4. The layer geometry and material properties used in the pressurized crack problems. The crack location at $0.5 < y < 3.5$ m is indicated by a thick black line and the crack is subjected to a normal stress of 10 MPa.

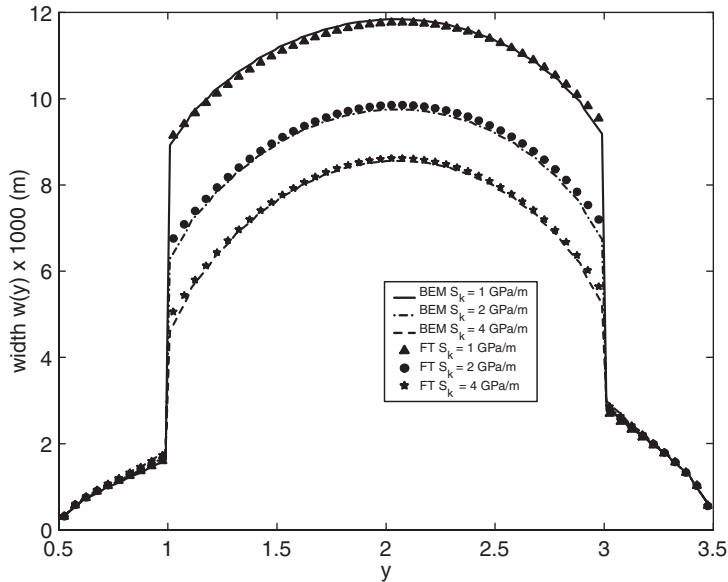


Figure 5. Fracture widths for cracks pressurized by 10 MPa, which intersect the three layers that are coupled by linear springs. Results are shown for the three different cases in which the interface spring stiffnesses are $S_i = 1, 2$, and 4 GPa/m . The FT Green's function solution using 60 piecewise constant DD elements to discretize the crack is compared with a BEM solution in which 2730 piecewise linear DD elements have been used to discretize the crack and the layer interfaces.

soft springs, both the solutions exhibit sharp jumps in the width profile as the crack crosses the interfaces located at $y = 1$ and 3 m . The larger displacement in the center layer is due to the softer Young's modulus of 5 GPa , whereas the displacement in the upper layer, within which the modulus is 20 GPa , is slightly larger than that in the lower layer having a modulus of 50 GPa .

4.2. Field example

A hydraulic fracturing treatment was carried out in a formation at a moderate depth. There was no apparent stress barrier above the pay zone, but the radioactive tracer logs indicated limited fracture height. The bottom hole pressure calculated from the measured surface treatment pressure exceeded the overburden stress σ_{yy} during the treatment. It was thus considered that the created fracture was likely to have a T-shape: a vertical main body and a horizontal component connected at the top of the main body. The horizontal component would allow fracturing fluid to enter between the formation layers and the cohesion of the interface between the layers would be much reduced. The Renshaw and Pollard criterion (17) can then be applied as a first-order approximation. The P3D simulator with the interfacial slip developed here was used to study this field case.

Application of criterion (17) with a tensile strength $T_0 = 0$ and a coefficient of friction $\mu = 0.4$ predicts that the fracture will not penetrate the interface located at a depth of 1663 m , where the layer stresses for the criterion are $\sigma_{xx} = 38.37 \text{ MPa}$, and $\sigma_{yy} = 41.28 \text{ MPa}$, and the pore pressure is $p_0 = 17.9 \text{ MPa}$. In the layers where the main fracture body propagated, Young's moduli

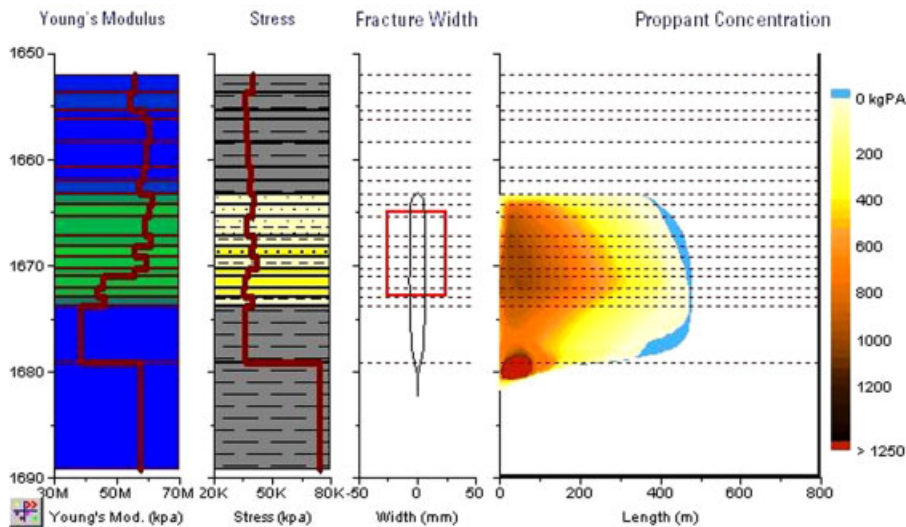


Figure 6. Fracture geometry from the simulation of a field example using the P3D simulator with interfacial slip.

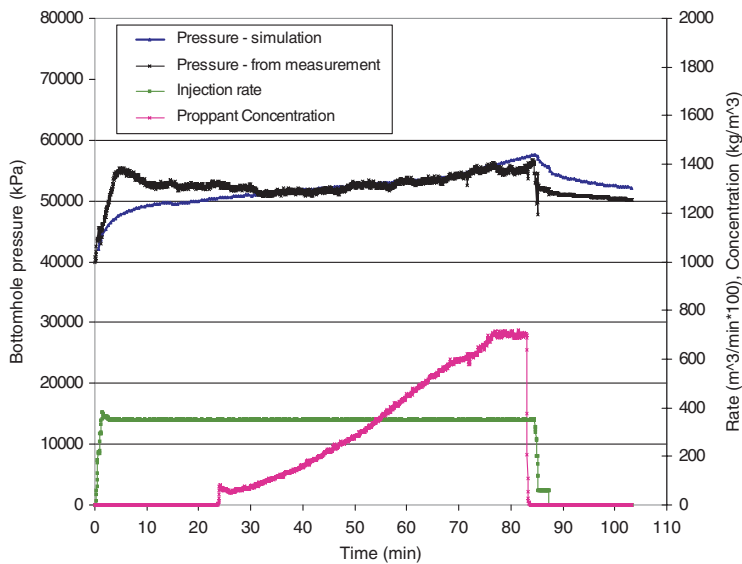


Figure 7. Comparison of bottom hole pressures from simulation and measurement.

ranged from 40–60 GPa. The bonded interfaces were allocated stiffness $S_i = 10$ GPa/m and the interface with a relative slip stiffness $S_i = 0.8$ GPa/m. Figure 6 shows the simulation results of fracture width profile, main fracture body with proppant concentration distribution, together with

the formation Young's modulus and the minimum horizontal *in situ* stress *versus* depth. The fracture height along the wellbore (at the origin of the length axis) is in good agreement with that determined from the radioactive tracer logs (not shown in the figure). The fracture's top tip shown in the width profile has a wide, blunt opening due to the interfacial slip, which is in contrast to the more familiar, conventional fracture tip as shown at the bottom of the fracture where there is no interfacial slip. Figure 7 compares the bottom hole fracturing pressure *versus* time between the simulation results and the measured data. Also shown in the figure are the injection rate and proppant concentration *versus* time that were recorded in the treatment and used in the simulation. Although the value of the shear stiffness of the interface with shear deformation was adjusted to match the magnitude of the measured pressure, a single value of the shear stiffness was used in the simulation for the entire treatment duration. There is good agreement between the pressure from the measurement and that from the simulation during most of the treatment. Due to the lack of measured material parameters comprising the coefficient of friction and the interface shear stiffness, the simulator is not yet a predictive model. This field case study indicates that interfacial slip could account for the fracture arrest at a layer interface as well as the fracturing pressure response during the treatment. The simulator does not currently account for the horizontal component of the T-shaped fracture. If the volume of fluid in the horizontal component is significant, the simulator will over-estimate the volume and length of the vertical main body of the fracture. On the other hand, a standard P3D simulation without interfacial slip would predict much larger fracture height than that determined from radioactive tracer logs.

5. CONCLUSIONS

In this paper we have presented a UAS that makes it possible to efficiently model cracks that touch or intersect interfaces between layered elastic media in which linear springs are assumed to control the shear deformation between the elastic layers. The assumption of linearity makes it possible to construct a spring layer Green's function that automatically incorporates the effects of the layer deformations. Assuming that the layers are parallel and that they have piecewise homogeneous elastic moduli, it is possible to construct the UAS very efficiently using the FT method. The UAS is constructed by superimposing the solution for a DD in a half-space that is joined by linear springs to another elastic half-space. When modeling cracks that touch or intersect interfaces, the source DDs introduce high wave number components into the spectral solution to multilayer problems that cannot be treated numerically. The UAS enables one to remove the high wave number components from the spectral solution for multiple-layer elastic problems leaving only low wave number components that need to be inverted numerically. Since these low wave number components are associated with modes whose spatial variation is moderate, they can be inverted and integrated with low-order Gauss integration. In this paper we have described the process by which the UAS can be constructed for 2D- and 3D-layered elastic media. The process of analytic integration of these singular solutions is also described.

For a problem comprising a pressurized crack intersecting two soft interfaces between three layers with different moduli, the numerical solution using the FT UAS algorithm with few degrees of freedom shows close agreement with a high-resolution BEM in which the crack and the layer interfaces are discretized. The UAS technique described in this paper was also used to generate a

layer Green's function for use in a P3D model of hydraulic fracturing. The Renshaw and Pollard criterion was first used to identify bonded interfaces and interfaces with slip, after which the appropriate layer stiffnesses were then allocated. Using these layer stiffnesses the associated layer Green's function table was assembled and used to model the increased fracture opening and reduced fluid pressures due to interface shear deformation for a hydraulic fracture that terminates on an interface. The results from the P3D model indicates that interface slip is able to account for the arrest of the fracture and the concomitant reduction in the fluid pressures that was observed in a field treatment.

APPENDIX A: FLEXIBILITY MATRICES

The explicit expressions for these flexibility sub-matrices for the s -subsystem are as follows:

$$R_{tt} = \frac{1}{D} \begin{bmatrix} -l_5(\text{th} + kd \cdot \text{se}^2) & -(l_4\text{th}^2 + fk^2d^2\text{se}^2) \\ -(l_4\text{th}^2 + fk^2d^2\text{se}^2) & -l_5(\text{th} - kd \cdot \text{se}^2) \end{bmatrix} \quad (\text{A1})$$

$$R_{bb} = \frac{1}{D} \begin{bmatrix} l_5(\text{th} + kd \cdot \text{se}^2) & -(l_4\text{th}^2 + fk^2d^2\text{se}^2) \\ -(l_4\text{th}^2 + fk^2d^2\text{se}^2) & l_5(\text{th} - kd \cdot \text{se}^2) \end{bmatrix} \quad (\text{A2})$$

$$R_{bt} = \frac{l_5}{D} \begin{bmatrix} -(\text{th} + kd)\text{se} & -kd \cdot \text{th} \cdot \text{se} \\ kd \cdot \text{th} \cdot \text{se} & -(\text{th} - kd)\text{se} \end{bmatrix} \quad (\text{A3})$$

$$R_{tb} = \frac{l_5}{D} \begin{bmatrix} (\text{th} + kd)\text{se} & -kd \cdot \text{th} \cdot \text{se} \\ kd \cdot \text{th} \cdot \text{se} & (\text{th} - kd)\text{se} \end{bmatrix} \quad (\text{A4})$$

where for the sake of brevity the superscript l identifying the layer number has been omitted and d is the thickness of the current layer. We have also used the notation $\text{th} = \tanh(kd)$, and $\text{se} = \operatorname{sech}(kd)$, and $D = f^2[(1 + k^2d^2)\text{se}^2 - 1]$. The explicit terms for the flexibility coefficients for the t -subsystem (for the t -system the R_{tt}, R_{bb}, \dots are numbers, not matrices) are as follows:

$$R_{tt} = \frac{2}{f} \coth(kd)$$

$$R_{bb} = -\frac{2}{f} \coth(kd)$$

$$R_{bt} = \frac{2}{f} \operatorname{cosech}(kd)$$

$$R_{tb} = -\frac{2}{f} \operatorname{cosech}(kd)$$

APPENDIX B: UAS COEFFICIENTS

The uniform asymptotic spectral coefficients $A_j^{l,Ps\mu}(k)$ that are calculated by substituting the expressions for $A_j^{l,PsU}(k)$, $A_j^{l,PsL}(k)$, and $A_j^{l,Ps\infty}(k)$ into (14) are given as follows:

$$\begin{aligned} A_1^{3,Ps\mu} &= g_1^{PL}(k) - g_3^{PU}(k), \quad A_2^{3,Ps\mu} = g_2^{PL}(k) + g_4^{PU}(k) \\ A_1^{2,Ps\mu} &= g_1^{PL}(k) - c_3, \quad A_2^{2,Ps\mu} = g_2^{PL}(k) + c_4 \\ A_3^{2,Ps\mu} &= -g_1^{PU}(k), \quad A_4^{2,Ps\mu} = g_2^{PU}(k) \\ A_1^{1,Ps\mu} &= g_1^{PL}(k), \quad A_2^{1,Ps\mu} = g_2^{PL}(k) \\ A_3^{1,Ps\mu} &= -g_1^{PU}(k) + c_3, \quad A_4^{1,Ps\mu} = g_2^{PU}(k) + c_4 \\ A_3^{0,Ps\mu} &= -g_1^{PU}(k) + g_3^{PL}(k), \quad A_4^{0,Ps\mu} = g_2^{PU}(k) + g_4^{PL}(k) \end{aligned} \quad (\text{B1})$$

Note that only the non-zero coefficients are listed. In addition, the g functions are defined as follows:

$$\begin{aligned} g_1^{PL}(k) &= g_1^P(k; \varepsilon_L, \delta_L, \sigma_L, \rho, h_L), \quad g_1^{PU}(k) = g_1^P(k; \varepsilon_U, \delta_U, \sigma_U, \rho, h_U) \\ g_2^{PL}(k) &= g_2^P(k; \varepsilon_L, \delta_L, \sigma_L, \rho, h_L), \quad g_2^{PU}(k) = g_2^P(k; \varepsilon_U, \delta_U, \sigma_U, \rho, h_U) \\ g_3^{PL}(k) &= g_3^P(k; \varepsilon_L, \delta_L, \sigma_L, \rho, h_L), \quad g_3^{PU}(k) = g_3^P(k; \varepsilon_U, \delta_U, \sigma_U, \rho, h_U) \\ g_4^{PL}(k) &= g_4^P(k; \varepsilon_L, \delta_L, \sigma_L, \rho, h_L), \quad g_4^{PU}(k) = g_4^P(k; \varepsilon_U, \delta_U, \sigma_U, \rho, h_U) \end{aligned}$$

where the functions $g_j^P(k; \varepsilon, \delta, \sigma, \rho, h)$ are defined as follows:

$$\begin{aligned} g_1^P(k; \varepsilon, \delta, \sigma, \rho, h) &= \frac{\alpha_1^1 k + \alpha_2^1 h k^2 + \alpha_3^1 h^2 k^3 + \sigma[\bar{\alpha}_0^1 + \bar{\alpha}_1^1(hk) + \bar{\alpha}_2^1(hk)^2]}{k + \beta\sigma} e^{-2kh} \\ g_2^P(k; \varepsilon, \delta, \sigma, \rho, h) &= \frac{\alpha_1^2 k + \alpha_2^2 h k^2 + \sigma[\bar{\alpha}_0^2 + \bar{\alpha}_1^2(hk)]}{k + \beta\sigma} e^{-2kh} \\ g_3^P(k; \varepsilon, \delta, \sigma, \rho, h) &= \frac{\alpha_1^3 k + \alpha_2^3 h k^2 + \alpha_3^3 h^2 k^3 + \sigma[\bar{\alpha}_0^3 + \bar{\alpha}_1^3(hk)]}{k + \beta\sigma} \\ g_4^P(k; \varepsilon, \delta, \sigma, \rho, h) &= \frac{\alpha_1^4 k + \alpha_2^4 h k^2 + \sigma\bar{\alpha}_0^4}{k + \beta\sigma} \end{aligned} \quad (\text{B2})$$

and the constants α_j^i and c_j are defined as follows:

$$\alpha_3^1 = 2\varepsilon(1+\rho)^2(2\varepsilon+\rho\delta)/\Delta_1$$

$$\alpha_2^1 = -2\varepsilon(1+\rho)[(1+\varepsilon)\delta\rho^2 + (\varepsilon^2 + 2\varepsilon + 2\varepsilon\delta)\rho + 2\varepsilon^2]/\Delta_1$$

$$\alpha_1^1 = -\varepsilon[\delta(1-\varepsilon)\rho^3 + (5\delta + 2\varepsilon - 2\varepsilon\delta + \varepsilon^2)\rho^2 + (10\varepsilon + 4\delta - 2\varepsilon^2)\rho + 8\varepsilon]/\Delta_1$$

$$\bar{\alpha}_2^1 = (1+\rho)^2(1-\varepsilon)[\varepsilon^2 + 3\varepsilon + \rho\varepsilon\delta + \rho\delta]/\Delta_1$$

$$\begin{aligned}
\bar{\alpha}_1^1 &= -\rho(1+\rho)(1-\varepsilon)[\varepsilon^2 + 3\varepsilon + \rho\varepsilon\delta + \rho\delta]/\Delta_1 \\
\bar{\alpha}_0^1 &= \frac{1}{2}[\delta(\varepsilon^2 - 1)\rho^3 + (\varepsilon^3 + 3\varepsilon^2\delta + 4\varepsilon^2 - 3\varepsilon - 5\delta)\rho^2 \\
&\quad + (3\varepsilon^3 + 16\varepsilon^2 - 15\varepsilon - 4\delta)\rho + 12\varepsilon(\varepsilon - 1)]/\Delta_1 \\
\alpha_2^2 &= 2\varepsilon(1+\rho)^2(2\varepsilon + \rho\delta)/\Delta_1 \\
\alpha_1^2 &= -\varepsilon(1+\rho)[\delta(\varepsilon + 3)\rho^2 + (\varepsilon^2 + 2\varepsilon\delta + 3\delta + 6\varepsilon)\rho + 2\varepsilon(\varepsilon + 3)]/\Delta_1 \\
\bar{\alpha}_1^2 &= (1+\rho)^2(1-\varepsilon)[\varepsilon^2 + 3\varepsilon + \rho\varepsilon\delta + \rho\delta]/\Delta_1 \\
\bar{\alpha}_0^2 &= -\frac{3}{2}(1-\varepsilon)(1+\rho)^2[\varepsilon^2 + 3\varepsilon + \rho\varepsilon\delta + \rho\delta]/\Delta_1 \\
\alpha_3^3 &= -2\varepsilon(1+\rho)(\varepsilon + \rho\delta)/\Delta_0 \\
\alpha_2^3 &= 2\varepsilon(1+\rho)(3\varepsilon + 2\rho\delta)/\Delta_0 \\
\alpha_1^3 &= -2\varepsilon[\delta\rho^2 + (2\varepsilon + \delta)\rho + 2\varepsilon]/\Delta_0 \tag{B3} \\
\bar{\alpha}_1^3 &= 2\varepsilon[(1-\delta)\rho + (1-\varepsilon)]/\Delta_0 \\
\bar{\alpha}_0^3 &= -[\delta(1+\varepsilon)\rho^2 + (3\varepsilon + \delta)\rho + 3\varepsilon(1-\varepsilon)]/\Delta_0 \\
\alpha_2^4 &= -2\varepsilon(1+\rho)(\varepsilon + \rho\delta)/\Delta_0 \\
\alpha_1^4 &= 2\varepsilon(1+\rho)(\varepsilon + \rho\delta)/\Delta_0 \\
\bar{\alpha}_0^4 &= -(1+3\varepsilon + (1+\varepsilon)\rho)(\varepsilon + \rho\delta)/\Delta_0 \\
\beta &= (\varepsilon^2 + 3\varepsilon + (1+\varepsilon)\rho\delta)(1+3\varepsilon + (1+\varepsilon)\rho)/\Delta_0 \\
\Delta_1 &= 2(2+\rho)\varepsilon[\delta(1+\varepsilon)\rho^2 + (\delta + 2\varepsilon\delta + 2\varepsilon + \varepsilon^2)\rho + 2\varepsilon(1+\varepsilon)] \\
\Delta_0 &= \Delta_1/(2+\rho) \\
c_3 &= -\frac{\rho}{2(2+\rho)} \\
c_4 &= -\frac{1+\rho}{2(2+\rho)}
\end{aligned}$$

The constants $\varepsilon_L, \delta_L, \sigma_L, \varepsilon_U, \delta_U, \sigma_U$, and ρ are defined as follows:

$$\varepsilon_L = \frac{G_1}{G_2}, \quad \delta_L = \frac{\lambda_1}{\lambda_2}, \quad \sigma_L = \frac{S_1}{G_2}, \quad \varepsilon_U = \frac{G_3}{G_2}, \quad \delta_U = \frac{\lambda_3}{\lambda_2}, \quad \sigma_U = \frac{S_2}{G_2} \quad \text{and} \quad \rho = \frac{\lambda_2}{G_2}$$

The uniform asymptotic spectral coefficients $A_j^{l,As\mu}(k)$ that are calculated by substituting $A_j^{l,AsU}(k)$, $A_j^{l,AsL}(k)$, and $A_j^{l,As\infty}(k)$ into (14) are given as follows:

$$\begin{aligned} A_1^{3,As\mu} &= g_1^{AL}(k) - g_3^{AU}(k), \quad A_2^{3,As\mu} = g_2^{AL}(k) + g_4^{AU}(k) \\ A_1^{2,As\mu} &= g_1^{AL}(k), \quad A_2^{2,As\mu} = g_2^{AL}(k) - c_4 \\ A_3^{2,As\mu} &= -g_1^{AU}(k), \quad A_4^{2,As\mu} = g_2^{AU}(k) \\ A_1^{1,As\mu} &= g_1^{AL}(k), \quad A_2^{1,As\mu} = g_2^{AL}(k) \\ A_3^{1,As\mu} &= -g_1^{AU}(k), \quad A_4^{1,As\mu} = g_2^{AU}(k) - c_4 \\ A_3^{0,As\mu} &= -g_1^{AU}(k) + g_3^{AL}(k), \quad A_4^{0,As\mu} = g_2^{AU}(k) + g_4^{AL}(k) \end{aligned} \tag{B4}$$

where

$$\begin{aligned} g_1^{AL}(k) &= g_1^A(k; \varepsilon_L, \delta_L, \sigma_L, \rho, h_L), \quad g_1^{AU}(k) = g_1^A(k; \varepsilon_U, \delta_U, \sigma_U, \rho, h_U) \\ g_2^{AL}(k) &= g_2^A(k; \varepsilon_L, \delta_L, \sigma_L, \rho, h_L), \quad g_2^{AU}(k) = g_2^A(k; \varepsilon_U, \delta_U, \sigma_U, \rho, h_U) \\ g_3^{AL}(k) &= g_3^A(k; \varepsilon_L, \delta_L, \sigma_L, \rho, h_L), \quad g_3^{AU}(k) = g_3^A(k; \varepsilon_U, \delta_U, \sigma_U, \rho, h_U) \\ g_4^{AL}(k) &= g_4^A(k; \varepsilon_L, \delta_L, \sigma_L, \rho, h_L), \quad g_4^{AU}(k) = g_4^A(k; \varepsilon_U, \delta_U, \sigma_U, \rho, h_U) \end{aligned}$$

and where the functions $g_j^A(k; \varepsilon, \delta, \sigma, \rho, h)$ are defined as follows:

$$\begin{aligned} g_1^A(k; \varepsilon, \delta, \sigma, \rho, h) &= \frac{\beta_1^1 k + \beta_2^1 h k^2 + \beta_3^1 h^2 k^3 + \sigma [\bar{\beta}_0^1 + \bar{\beta}_2^1 (h k)^2]}{k + \beta \sigma} e^{-2kh} \\ g_2^A(k; \varepsilon, \delta, \sigma, \rho, h) &= \frac{\beta_1^2 k + \beta_2^2 h k^2 + \sigma [\bar{\beta}_0^2 + \bar{\beta}_1^2 (h k)]}{k + \beta \sigma} e^{-2kh} \\ g_3^A(k; \varepsilon, \delta, \sigma, \rho, h) &= \frac{\beta_1^3 k + \beta_2^3 h k^2 + \beta_3^3 h^2 k^3 + \sigma [\bar{\beta}_0^3 + \bar{\beta}_1^3 (h k)]}{k + \beta \sigma} \\ g_4^A(k; \varepsilon, \delta, \sigma, \rho, h) &= \frac{\beta_1^4 k + \beta_2^4 h k^2 + \sigma \bar{\beta}_0^4}{k + \beta \sigma} \end{aligned} \tag{B5}$$

Here the constants c_4 and β_j^i are defined as follows:

$$\beta_3^1 = -2\varepsilon(1+\rho)^2(2\varepsilon+\rho\delta)/\Delta_1$$

$$\beta_2^1 = 2\varepsilon^2(1+\rho)(2+\rho)(\varepsilon+\rho\delta)/\Delta_1$$

$$\beta_1^1 = 2\varepsilon(2+\rho)(2\varepsilon+\rho\delta)/\Delta_1$$

$$\bar{\beta}_2^1 = (1+\rho)^2(\varepsilon-1)(\varepsilon^2+3\varepsilon+\rho\varepsilon\delta+\rho\delta)/\Delta_1$$

$$\bar{\beta}_0^1 = -(2+\rho)(3\varepsilon^2-3\varepsilon-\rho\delta+\varepsilon^2\rho)/\Delta_1$$

$$\begin{aligned}
\beta_2^2 &= -2\varepsilon(1+\rho)^2(2\varepsilon+\rho\delta)/\Delta_1 \\
\beta_1^2 &= \varepsilon(1+\rho)[\delta(\varepsilon+1)\rho^2+(\varepsilon^2+2\varepsilon\delta+3\delta+2\varepsilon)\rho+2\varepsilon(\varepsilon+3)]/\Delta_1 \\
\bar{\beta}_1^2 &= (\varepsilon-1)(1+\rho)^2(\varepsilon^2+3\varepsilon+\rho\varepsilon\delta+\rho\delta)/\Delta_1 \\
\bar{\beta}_0^2 &= -\frac{1}{2}(\varepsilon-1)(1+\rho)(3+\rho)(\varepsilon^2+3\varepsilon+\rho\varepsilon\delta+\rho\delta)/\Delta_1 \\
\beta_3^3 &= 2\varepsilon(1+\rho)(\varepsilon+\rho\delta)/\Delta_0 \\
\beta_2^3 &= -2\varepsilon(3\varepsilon+2\rho\delta+2\rho\varepsilon+\delta\rho^2)/\Delta_0 \\
\beta_1^3 &= 2\varepsilon(\delta\rho+2\varepsilon)/\Delta_0 \\
\bar{\beta}_1^3 &= 2\varepsilon(\varepsilon+\delta\rho-\rho-1)/\Delta_0 \\
\bar{\beta}_0^3 &= -(3\varepsilon^2-3\varepsilon-\rho\delta+\varepsilon^2\rho)/\Delta_0 \\
\beta_2^4 &= 2\varepsilon(1+\rho)(\varepsilon+\rho\delta)/\Delta_0 \\
\beta_1^4 &= -2\varepsilon(\varepsilon+\rho\delta)/\Delta_0 \\
\bar{\beta}_0^4 &= (\varepsilon+\rho\delta)(1+3\varepsilon+\rho(1+\varepsilon))/\Delta_0 \\
\beta &= (\varepsilon^2+3\varepsilon+(1+\varepsilon)\rho\delta)(1+3\varepsilon+(1+\varepsilon)\rho)/\Delta_0 \\
\Delta_1 &= 2(2+\rho)\varepsilon[\delta(1+\varepsilon)\rho^2+(\delta+2\varepsilon\delta+2\varepsilon+\varepsilon^2)\rho+2\varepsilon(1+\varepsilon)] \\
\Delta_0 &= \Delta_1/(2+\rho) \\
c_4 &= -\frac{1+\rho}{2(2+\rho)}
\end{aligned} \tag{B6}$$

The uniform asymptotic spectral coefficients $A_j^{l,At\mu}(k)$ that are calculated by substituting $A_j^{l,AtU}(k)$, $A_j^{l,AtL}(k)$, and $A_j^{l,At\infty}(k)$ into (14) are given as follows:

$$\begin{aligned}
A_5^{3,At\mu} &= g_1^{TL}(k) + g_2^{TU}(k) \\
A_5^{2,At\mu} &= 1 + g_1^{TL}(k), \quad A_6^{2,At\mu} = g_1^{TU}(k) \\
A_5^{1,At\mu} &= g_1^{TL}(k), \quad A_6^{1,At\mu} = 1 + g_1^{TU}(k) \\
A_6^{0,At\mu} &= g_1^{TU}(k) + g_2^{TL}(k)
\end{aligned} \tag{B7}$$

where

$$\begin{aligned}
g_1^{TL}(k) &= g_1^T(k; \varepsilon_L, \sigma_L, h_L), \quad g_1^{TU}(k) = g_1^T(k; \varepsilon_U, \sigma_U, h_U) \\
g_2^{TL}(k) &= g_2^T(k; \varepsilon_L, \sigma_L, h_L), \quad g_2^{TU}(k) = g_2^T(k; \varepsilon_U, \sigma_U, h_U)
\end{aligned}$$

and

$$g_1^T(k; \varepsilon, \sigma, h) = \frac{k + \sigma \bar{\gamma}_0^1}{k + \beta_T \sigma} e^{-2kh}$$

$$g_2^T(k; \varepsilon, \sigma, h) = \frac{\sigma \bar{\gamma}_0^2}{k + \beta_T \sigma}$$

where $\bar{\gamma}_0^1 = (1 - \varepsilon)/\varepsilon$, $\bar{\gamma}_0^2 = 2/\varepsilon$, and $\beta_T = (1 - \varepsilon)/\varepsilon$ and $\bar{\gamma}_q^{PL}$ and $\bar{\gamma}_q^{PU}$ are obtained by using the values of ε_L and ε_U , respectively.

If we consider the limit $\sigma_j \rightarrow \infty$ for all three types of coefficients P_s , A_s , and A_t we recover the coefficients [6] that were obtained for the fully bonded interfaces. This is to be expected since the limit $\sigma_j = S_j/G_2 \rightarrow \infty$ corresponds to infinitely stiff interface springs so that the interfaces become fully bonded in the limit.

APPENDIX C: INTEGRALS FOR THE REMAINDER TERM

In this section we list the integrals required to determine the integrated kernels for the UAS associated with a constant DD. We introduce the notation

$$K_{-1n} = \int e^s E_1(s) s^n ds$$

for which the explicit expressions for $n = 0, 1, 2$ are

$$K_{-10} = e^s E_1(s) + \ln s$$

$$K_{-11} = (s - 1)e^s E_1(s) + s - \ln s$$

$$K_{-12} = (s^2 - 2s + 2)e^s E_1(s) + \frac{s^2}{2} - 2s + 2\ln s$$

ACKNOWLEDGEMENTS

The authors wish to thank Schlumberger for permission to publish this work. In addition, the authors wish to thank Dr J. A. L. Napier for useful discussions and for running some test models.

REFERENCES

1. Salamon MD. Subsidence prediction using a laminated linear model. In *Rock Mechanics as a Guide for Efficient Utilization of Natural Resources*, Khair (ed.). Balkema: Rotterdam, 1998.
2. Yue ZQ, Yin J-H. Backward transfer-matrix method for elastic analysis of layered solids with imperfect bonding. *Journal of Elasticity* 1998; **50**:109–128.
3. Barree RD, Winterfield PH. Effects of shear planes and interfacial slip of fracture growth and treating pressures. *Paper SPE 48926 Presented at the 1998 SPE Annual Technical Conference and Exhibition*, New Orleans, 27–30 September 1998.
4. Wang X, Pan E. Exact solutions for simply supported and multilayered piezothermoelastic plates with imperfect interfaces. *The Open Mechanics Journal* 2007; **1**:1–10.
5. Crouch SL, Starfield AM. *Boundary Element Methods in Solid Mechanics*. Unwin Hyman: London, 1990.

6. Peirce AP, Siebrits E. Uniform asymptotic approximations for accurate modeling of cracks in layered elastic media. *International Journal of Fracture* 2001; **110**:205–239.
7. Peirce AP, Siebrits E. The scaled flexibility matrix method for the efficient solution of boundary value problems in 2D and 3D layered elastic media. *Computer Methods in Applied Mechanics and Engineering* 2001; **190**: 5935–5956.
8. Siebrits E, Peirce A. An efficient multi-layer planar 3D fracture growth algorithm using a fixed mesh approach. *International Journal for Numerical Methods in Engineering* 2002; **53**:691–717.
9. Renshaw CE, Pollard DD. An experimentally verified criterion for propagation across unbounded frictional interfaces in brittle, linear elastic materials. *International Journal of Rock Mechanics and Mining Sciences and Geomechanics Abstracts* 1995; **32**:237–249.
10. Wardle LJ. Stress analysis of multilayered anisotropic elastic systems subject to rectangular loads. *Technical Paper No. 33*, CSIRO Institute of Earth Resources, Division of Applied Geomechanics, Australia, 1980.
11. Buffler H. Theory of elasticity of a multilayered medium. *Journal of Elasticity* 1971; **1**(2):125–143.
12. Lin W, Keer LM. Analysis of a vertical crack in a multilayered medium. *Journal of Applied Mechanics (ASME)* 1989; **56**:63–69.
13. Lin W, Keer LM. Three-dimensional analysis of cracks in layered transversely isotropic media. *Proceedings of the Royal Society of London, Series A* 1989; **424**:307–322.
14. Pan E. Static Green's functions in multilayered half spaces. *Applied Mathematical Modelling* 1997; **21**:509–521.
15. Singh SJ. Static deformation of a multilayered half-space by internal sources. *Journal of Geophysical Research* 1970; **75**:3257–3263.
16. Singh SJ. Static deformation of a transversely isotropic multilayered half-space by surface loads. *Physics of the Earth and Planetary Interiors* 1986; **42**:263–273.
17. Sneddon IN. *Fourier Transforms*. Dover: New York, NY, 1995.
18. Linkov A, Filippov N. Difference equations approach to the analysis of layered systems. *Meccanica* 1991; **26**:195–209.
19. Kennet BLN. *Seismic Wave Propagation in Stratified Media*. Cambridge University Press: Cambridge, 1983.
20. Bender CM, Orszag SA. *Advanced Mathematical Methods for Scientists and Engineers*. McGraw-Hill: New York, NY, 1978.
21. Siebrits E, Gu H, Desroches J. An improved pseudo-3D hydraulic fracturing simulator for multiple layered materials. In *Computer Methods and Advances in Geomechanics*, Desai CS et al. (eds). *Proceedings of the 10th International Conference on Computer Methods and Advances in Geomechanics (IACMAG)*, Tucson, 7–12 January 2001. Balkema: Rotterdam, 2001; 1341–1345.
22. Napier JAL. Personal Communication, 2006.